Minimal current phase and universal boundary layers in driven diffusive systems

J. S. Hager,[1] J. Krug,[2,3] V. Popkov,[4,5] and G. M. Schütz[6]
[1]*Institut für Theoretische Physik, RWTH-Aachen, 52056 Aachen, Germany*
[2]*Fachbereich Physik, Universität GH Essen, D-45117 Essen, Germany*
[3]*Department of Physics and CAMP, Technical University of Denmark, DK-2800 Lyngby, Denmark*
[4]*Fachbereich Physik, Freie Universität Berlin, Arnimallee 14, D-14195 Berlin, Germany*
[5]*Institute for Low Temperature Physics, 310164 Kharkov, Ukraine*
[6]*Institut für Festkörperforschung, Forschungszentrum Jülich, D-52425 Jülich, Germany*
(Received 5 December 2000; published 16 April 2001)

We investigate boundary-driven phase transitions in open driven diffusive systems. The generic phase diagram for systems with short-ranged interactions is governed by a simple extremal principle for the macroscopic current, which results from an interplay of density fluctuations with the motion of shocks. In systems with more than one extremum in the current-density relation, one finds a minimal current phase even though the boundaries support a higher current. The boundary layers of the critical minimal current and maximal current phases are argued to be of a universal form. The predictions of the theory are confirmed by Monte Carlo simulations of the two-parameter family of stochastic particle hopping models of Katz, Lebowitz, and Spohn and by analytical results for a related cellular automaton with deterministic bulk dynamics. The effect of disorder in the particle jump rates on the boundary layer profile is also discussed.

DOI: 10.1103/PhysRevE.63.056110 PACS number(s): 64.60.Cn, 05.70.Ln, 02.50.Ga

I. INTRODUCTION

Imagine a driven particle system—it may be *any* system, such as ribosomes moving along an *m*-RNA, ions diffusing in a narrow channel, or even cars proceeding on a long road—where classical objects move with preference in one direction and which is coupled at its two ends to external reservoirs. Such a system with open boundaries where particles can enter and leave will maintain a nonequilibrium steady state that is characterized by some bulk density ρ and the corresponding particle current $j(\rho)$. There is no general notion such as a Gibbs measure that would, at least in principle, determine the statistical properties of the steady state, and also other more specialized approaches [1,2] to nonequilibrium behavior cannot predict into which bulk density the system will settle. However, it is intuitively clear that unlike in equilibrium systems, here boundaries will play a decisive part in determining the bulk behavior of the system: Since the system is open at the boundaries, particles will flow in, pass through the system, and finally flow out at the other boundary. Therefore, metaphorically speaking, the current will carry boundary effects into the bulk.

This consideration raises two distinct questions that we wish to address. The first concerns the bulk dynamics that link boundary properties with bulk properties. In continuation of previous work [3,4], we show in detail how local fluctuations and shocks determine an evolving nonstationary density profile and thus eventually lead to the stationary bulk density as a function of the given fixed boundary densities, i.e., the phase diagram of the system (Sec. II). We illustrate these mechanisms in a specific example, viz., a class of lattice-gas models introduced some years ago by Katz, Lebowitz, and Spohn [5]. Starting from such a mesoscopic viewpoint, our theoretical approach allows us then to make contact with an earlier phenomenological hydrodynamic approach [6,7] (Sec. III).

The second question concerns the properties of the stationary boundary layer. In Ref. [6], it was argued, on the basis of scaling considerations and supporting Monte Carlo simulations, that the density profile in the maximum current phase (where the bulk density becomes independent of the boundary conditions) decays towards its bulk limit as a power law with an exponent of $-\frac{1}{2}$. The universality of this power law was subsequently confirmed by exact solutions of various lattice-gas models [8–12] and a renormalization-group analysis of the corresponding stochastic field theory [13]. In Sec. IV, we present a refined version of the scaling argument of [6] that allows us to predict also the form of the prefactor, up to a universal amplitude that is extracted from the exact solutions, and verify this prediction by Monte Carlo simulations, described in Sec. V.

In Sec. VI, we introduce a cellular automaton with deterministic next-nearest-neighbor bulk interaction and open, stochastic boundary conditions. We investigate to which extent the theoretical scenario remains valid for this model. Section VII is devoted to the effects of quenched particle-wise disorder on the boundary-layer profile, and we conclude with some final remarks and open questions in Sec. VIII. Technical details for the derivation of some exact results are presented in the Appendixes.

We remark that one expects the topology of the boundary to play an important role in the study of a specific problem. However, when addressing the first question regarding the bulk mechanisms that carry the information, one may disregard this dependence. Since, furthermore (as it turns out), the nature of these mechanisms is independent of dimensionality, we restrict our discussion to the topologically simplest case of one-dimensional systems where the boundaries reduce to two single points. Natural examples for this setup are many-body systems such as those mentioned above, viz., where the dynamic degrees of freedom reduce to effectively one dimension as, e.g., in traffic flow [14–16], the kinetics of

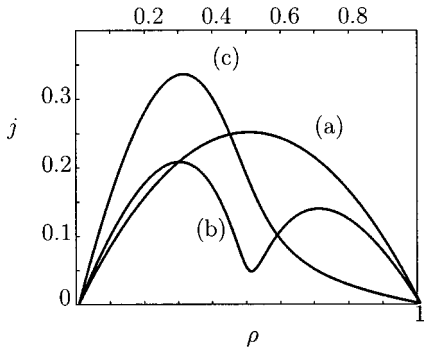

FIG. 1. Exact current-density relations of the KLS model plotted from the formula (A6). (a) $\epsilon=0.0$, $\delta=0$ (TASEP); (b) $\epsilon=0.995$, $\delta=0.2$, considered below; (c) $\epsilon=0.9$, $\delta=0.9$. The rates are defined in Eqs. (1)–(4).

protein synthesis [17,18], ionic diffusion in zeolites [19], or the motion of colloidal particles in narrow channels [20].

II. STEADY-STATE SELECTION

At first glance, the question of steady-state selection appears to be ill-posed as undoubtedly the answer to this problem depends on the system under investigation. However, for the case of vanishing right boundary density ($\rho_+=0$), Krug [6] postulated a rather general maximal-current principle that asserts that independent of the details of the dynamics, the system tries to maximize its stationary current j in the sense that $j=\max_{\rho\in[0,\rho-]} j(\rho)$. Here ρ_- is the constant density of the left reservoir from which particles are flowing into the system. (Without loss of generality, we shall always assume a bulk current to the right.)

The validity of the maximal-current principle was supported using phenomenological stability arguments and Monte Carlo simulations of a nonequilibrium kinetic Ising model introduced by Katz, Lebowitz, and Spohn [5]. We shall refer to this model as the KLS model. This is an exclusion process in which each lattice site may be occupied by at most one particle. Particles hop randomly (with some bias) to their nearest-neighbor sites with rates depending on the occupation of the nearest- and next-nearest-neighbor site. In the totally asymmetric case, particles hop only to the right with bulk hopping rates

$$0\ 1\ 0\ 0 \to 0\ 0\ 1\ 0 \quad \text{with rate } 1+\delta, \tag{1}$$

$$1\ 1\ 0\ 0 \to 1\ 0\ 1\ 0 \quad \text{with rate } 1+\epsilon, \tag{2}$$

$$0\ 1\ 0\ 1 \to 0\ 0\ 1\ 1 \quad \text{with rate } 1-\epsilon, \tag{3}$$

$$1\ 1\ 0\ 1 \to 1\ 0\ 1\ 1 \quad \text{with rate } 1-\delta, \tag{4}$$

where $|\epsilon|<1$, $|\delta|<1$. Here ''1'' marks the occupation of a lattice site by a particle. The stationary current $j(\rho)$ (Fig. 1) can be computed exactly from the stationary measure of the periodic system, which is the equilibrium distribution of the one-dimensional Ising model (see Appendix A). For $\delta=0$, this computation was first carried out by Brandstetter [21] (see also [6,22]).

For sufficiently strong repulsive interaction ($1-\epsilon\ll 1$), the current at half-filling is strongly suppressed, which brings about a two-maxima structure in the current-density relation. The limit $\epsilon=1$ leads to $j_{\min}=0$. Varying $0\leqslant\epsilon\leqslant 1$ interpolates between a single maximum of the current and the double-hump structure. The other parameter, δ, is responsible for the particle-hole asymmetry. $\delta=0$ corresponds to a symmetric graph $j(\rho)=j(1-\rho)$. $\delta\neq 0$ breaks the particle-hole symmetry in favor of a larger particle current ($\delta>0$) or larger vacancy current ($\delta<0$). For negative ϵ (attractive interaction), the current-density relation always has a single maximum. The special case $\epsilon=\delta=0$ is an exactly solvable model known as the totally asymmetric simple exclusion process (TASEP) [23–25]. For this model, the stationary current as a function of the particle density is given by $j(\rho)=\rho(1-\rho)$. Also the phase diagram of the open system is known exactly [26,8,9]. The case $\epsilon=\delta$ is a simple model for traffic flow, which has been studied in detail in [27].

To study the effect of open boundaries, we imagine the left boundary of the system (where particles are injected) to be coupled to a reservoir of constant density $\hat{\rho}_-$. At the right boundary, particles hop into a reservoir of constant density $\hat{\rho}_+$. The rates of particle injection and absorption at the boundaries are specified below. They are chosen such that the reservoir densities induce effective boundary densities $\rho_\pm$ in the system of the same magnitude. We use this model for illustration and numerical and analytical verification of our results on the phase diagram (i.e., the bulk density ρ as function of the boundary densities $\rho_\pm$) and on the shape of the stationary density profile.

Using insights gained from the exact solution of the TASEP [8], it was shown [3,4] how rather general dynamical properties of driven diffusive systems lead to a phase diagram governed by the extremal principle,

$$j=\begin{cases} \max\limits_{\rho\in[\rho_+,\rho_-]} j(\rho) & \text{for } \rho_->\rho_+ \\ \min\limits_{\rho\in[\rho_-,\rho_+]} j(\rho) & \text{for } \rho_-<\rho_+ \end{cases}. \tag{5}$$

The microscopic details of the system enter only in so far as they determine the functional form of the current $j(\rho)$ and the effective boundary densities $\rho_+(\hat{\rho}_+)$, $\rho_-(\hat{\rho}_-)$ which depend on the actual reservoir densities $\hat{\rho}_\pm$ through the details of the coupling mechanism. The first relation is an extension of Krug's current maximization principle and reduces to it for $\rho_+=0$. It was first suggested by Janssen and Oerding [28]. The second relation is somewhat surprising. It states that the system tends to *minimize* its current if the density gradient $\rho_+-\rho_-$, set by the boundaries, is positive.

A. Phase diagrams

The order parameter that characterizes the selected steady state is the bulk density. The structure of the phase diagram, which exhibits a variety of first- and second-order nonequilibrium transitions, is determined by the number of extrema of the current. For systems with a single maximum in the current at some density ρ^*, the phase diagram has three

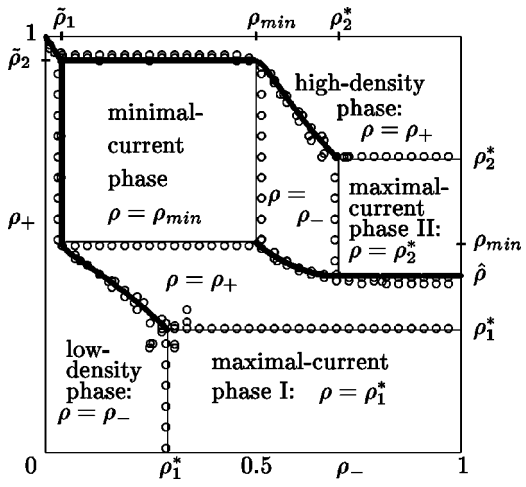

FIG. 2. Phase diagram of the KLS model with two maxima at $\rho^*_{1,2}$ and a minimum at $\rho_{\min}=0.5$ in the current density relation [4]. Full (bold) lines indicate phase transitions of second (first) order, calculated from Eq. (5). Circles show the results of Monte Carlo simulations of a system with 150 sites (see below).

phases: a maximal-current phase C in the domain $\rho_-<\rho^*$, $\rho_+<\rho^*$ (bulk density $\rho=\rho^*$), with second-order transitions to the low-density ($\rho=\rho_-<\rho^*$) and the high-density phase ($\rho=1-\rho_+>\rho^*$), respectively. These phases are separated by a first-order transition along the line $j(\rho_-)=j(\rho_+)$ in the domain $\rho_-<\rho^*$, $\rho_+>\rho^*$.

In a system with two maxima in the current-density relation, one also finds maximal-current phases and low- and high-density phases, respectively, separated by first- and second-order transition lines. However, the minimization principle for the current brings about a phase of a rather unexpected nature: In the range of boundary densities defined by

$$j(\rho_+),j(\rho_-)>j(\rho_{\min}),\quad \rho_-<\rho_{\min}<\rho_+, \tag{6}$$

the system organizes itself into a state with bulk density $\rho_{\rm bulk}$ corresponding to the local minimum of the current even though both boundary densities support a higher current. We shall refer to this phase as the *minimal current phase*. Generally, for a system with two maxima of the current, the phase diagram consists of seven distinct phases, including two maximal current phases with bulk densities corresponding to the respective maxima of the current and the minimal current phase (Fig. 2).

B. Stability and branching of shocks

To understand the origin of the phase diagram, we first recall that in the absence of detailed balance, stationary behavior cannot be understood in terms of a free energy, but has to be derived from the system dynamics. Following Kolomeisky *et al.* [3], there are two basic dynamical phenomena to consider, namely shocks and the diffusive motion of localized density waves.

A shock in a system of classical flowing particles is a nonequilibrium domain wall that marks the sudden transition from a stationary region of low density to a stationary region

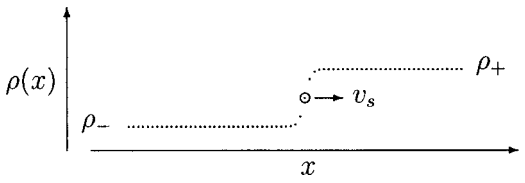

FIG. 3. Motion of a shock in an ensemble average of the lattice gas. To the left (right) of the domain wall, particles are distributed homogeneously with an average density ρ_- (ρ_+) on each lattice site. The corresponding stationary currents $j_\pm$ determine the drift velocity v_s [Eq. (7)] of the shock.

of high density (see Fig. 3). A well-known example for a shock is the beginning of a traffic jam on a motorway where incoming cars (almost freely flowing particles in the low-density regime) have to slow down very quickly over a short distance and then form part of the (high-density) congested region. A remarkable feature of such shocks is their long-time stability, i.e., they remain localized over distances comparable to the size of particles. In some sense one may regard shocks as solitonlike collective excitations of the particle system [29]. Irrespective of the specific system, mass conservation yields the shock velocity

$$v_s=\frac{j_+-j_-}{\rho_+-\rho_-}, \tag{7}$$

where $\rho_\pm$ are the shock densities and $j_\pm\equiv j(\rho_\pm)$ are the corresponding currents to the left ($-$) and to the right ($+$) of the shock, respectively.

A second characteristic velocity describes the motion of a density wave, i.e., a localized perturbation in a stationary region of background density ρ (Fig. 4). Such a perturbation spreads out and slowly decays in the course of time, but keeps a constant center-of-mass velocity v_c. Under mild assumptions on the nature of the steady state, this collective velocity is given by the derivative

$$v_c=\frac{\partial}{\partial\rho}j \tag{8}$$

of the stationary current [24].

The velocities (7) and (8) and the underlying single-shock picture are sufficient to understand the phase diagram of systems with a single maximum in the current [3]. A change of sign in the shock velocity v_s marks a first-order transition between the low- and high-density phases, whereas a change of sign in the collective velocity v_c signals a second-order transition to the maximal-current phase. If the current has a

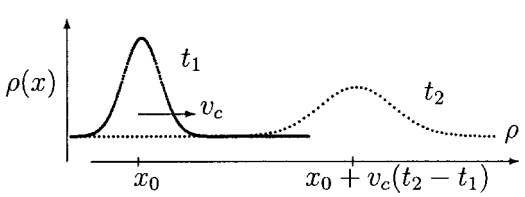

FIG. 4. Diffusive spreading of a density perturbation in the steady state at two times $t_2>t_1$. The collective velocity describes the motion of the center of mass of the perturbation.

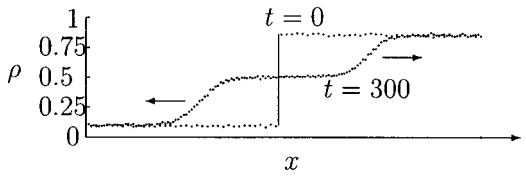

FIG. 5. Monte Carlo simulation of the particle density distribution in a lattice gas in the initial state (one shock) and after 300 Monte Carlo sweeps, showing branching into two shocks. 3000 histories are averaged over [4].

local minimum, it was argued in a qualitative manner how a single shock may branch into two distinct shocks, moving away from each other (Fig. 5), and thus lead to the occurrence of the minimal-current phase [4]. Here we describe in detail how the branching mechanism and the resulting structure of the shocks follows from the stability criterion,

$$v_c(\rho_D) > v_s(\rho_L, \rho_R) > v_c(\rho_R) \tag{9}$$

for a single shock, which one obtains by considering the flow of fluctuations in the neighborhood of the shock [24].

Consider the time evolution of a judiciously chosen shock initial state. Because of ergodicity, the steady state does not depend on the initial conditions and a specific choice involves no loss of generality. It is convenient to consider an initial configuration with a shock with densities ρ_- and ρ_+ on the left and on the right, respectively, which is composed of many narrow subsequent shocks at various levels of intermediate densities (Fig. 6). The left density ρ_- is supposed to be less than the density $\rho_{\min}$ where the current has a local minimum, while ρ_+ is taken as larger than $\rho_{\min}$.

From the convexity condition (9), one reads off which of these ''minishocks'' are stable while Eq. (7) yields the respective shock velocity. Consider now the minimal-current regime defined by Eq. (6). We define as $\sigma_\pm$ the two inflection points of the current-density relation between the two maxima of the current. For $\rho_- < \sigma_-$ and $\rho_+ > \sigma_+$, one finds the following.

(i) There are densities $\rho_u > \rho_{\min}$ and $\rho_l < \rho_{\min}$ such that the two sets of minishocks which have (a) $\rho_-^{(n)} > \rho_u$ and (b) $\rho_+^{(k)} < \rho_l$, respectively, are stable.

(ii) All mini shocks in the set (a) move to the right while all mini shocks in the set (b) move to the left.

(iii) The shock velocities in the two sets of stable minishocks are such that they all catch up with the respective slowest one and thus eventually coalesce into two distinct single large shocks with boundary densities (ρ_-, ρ_l) (moving to the left) and (ρ_u, ρ_+) (moving to the right), respectively.

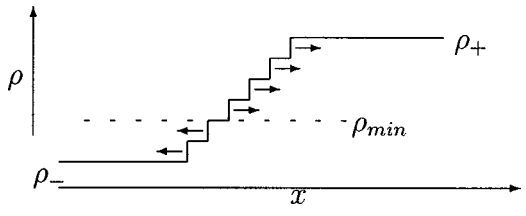

FIG. 6. Schematical drawing of small shocks and their velocities, leading to branching and coalescence. Each ''minishock'' has left and right boundary densities $\rho_\pm^{(k)}$ in the interval $\rho_- \leqslant \rho_-^{(k)}$ and $\rho_+^{(n)} \leqslant \rho_+$, respectively. The boundary densities $\rho_\pm$ are within the minimal-current regime (6).

This leads to the branching of the single (composite) shock into two distinct, oppositely moving shocks. The values $\rho_{u,l}$ depend on $\rho_\pm$ through the stability criterion (9). Notice that the composition into subsequent minishocks is just a tool to visualize the mechanism leading to the branching. One may always set the imagined length of the minishocks to zero to obtain the same prediction for the time evolution of a single shock. This is confirmed by the simulation data shown in Fig. 5. The coalescence of shocks within each branch of the pair of oppositely moving shocks is analogous to the phenomenon of coalescence, which has been proved rigorously to take place in the TASEP on the hydrodynamic scale [30] (see below). Notice that because of the diffusive fluctuations in the shock position, the shock at time $t > 0$ does not appear in Fig. 5 as a sharp increase of the density.

It remains to discuss the behavior of the unstable shocks. We consider the shocks $(\rho_-^{(n)}, \rho_+^{(n)})$ with $\rho_-^{(n)} \geqslant \rho_{\min}$ and $\rho_+^{(n)} \leqslant \rho_u$. By taking the limit of infinitesimal shock height $\varepsilon = \rho_+^{(n)} - \rho_-^{(n)}$, one obtains as ''velocity'' of these infinitesimal unstable shocks the collective velocity $u_c(\rho_-^{(n)})$. Thus infinitesimal shocks move with the speed of perturbations. Going to the scaling limit $x, t \to \infty$ (with $u = x/t$ fixed), diffusive (and even superdiffusive) fluctuations are scaled out and there remains only a large-scale description of the evolving density profile in terms of points u representing the unstable minishocks. Hence on this scale a point with density ρ moves with velocity $v_c(\rho)$. This observation leads to a hydrodynamic description of the large-scale dynamics discussed in the following section.

III. HYDRODYNAMIC APPROACH

Because of particle number conservation, the local density of a driven diffusive system with nearest-neighbor hopping satisfies a lattice continuity equation of the type

$$\frac{d}{dt}\rho_k = j_{k-1} - j_k, \tag{10}$$

where j_k is the expectation value of the current across a bond $(k, k+1)$. For the KLS model, it is given by

$$\begin{aligned} j_k = {} & (1+\delta)\langle 0100\rangle + (1+\epsilon)\langle 1100\rangle \\ & + (1-\epsilon)\langle 0101\rangle + (1-\delta)\langle 1101\rangle \end{aligned} \tag{11}$$

evaluated at the four neighboring sites $(k-1, k, k+1, k+2)$. The lattice continuity equation does not admit an explicit solution: In order to integrate Eq. (10), one would have to write down the equations of motion for the currents (which involve five-point correlation functions) and would eventually end up with an infinite hierarchy of coupled equations for n-point correlation functions.

On the other hand, according to the previous discussion, one can construct the time evolution of a nonstationary den-

sity profile on the Euler scale $k,t\to\infty$ with $u=k/t$ fixed. There are shock discontinuities with a range of stability defined by Eq. (9). A shock (ρ_-,ρ_+) is stable if the convexity condition (9) for the current is met in the full interval $[\rho_-,\rho_+]$. (The diffusive nature of the shock position does not appear on this scale.) Outside the range of stability, the prescription for the construction of the density profile $\rho \equiv \rho(u)$ yields the implicit relation

$$u = v_c(\rho). \tag{12}$$

Notice that this is nothing but the scaling solution of the continuum limit

$$\frac{\partial}{\partial t}\rho = -\frac{\partial}{\partial x} j \tag{13}$$

of the continuity equation (10). Here $j \equiv j(\rho)$ is the stationary current across a bond at density ρ, which for the KLS model is given in Appendix A. Setting $u=x/t$ then yields Eq. (12). On this hydrodynamical scale, the stability criterion of the shock becomes the definition of a shock discontinuity for the weak solutions of the Cauchy problem defined by Eq. (13), together with the initial condition $\rho(x,0)=\rho_0(x)$ (see [33] for a full discussion).

One may go further and try to adapt this insight to the derivation of the stationary solution of a finite system with fixed boundary densities $\rho_\pm$. Following Refs. [6,7], we postulate a diffusive excess current $j_{\rm ex} = -\nu(\partial\rho/\partial x)$, which is to be added to the continuity equation (13), which then reads

$$\frac{\partial}{\partial t}\rho = -\frac{\partial}{\partial x} J \tag{14}$$

with $J = j - \nu\rho'$. The stationarity condition takes the form

$$J = \text{const} \equiv j^* \tag{15}$$

with boundary conditions

$$\rho(0)=\rho_-, \quad \rho(L)=\rho_+. \tag{16}$$

This may be integrated and one obtains

$$\int_{\rho_-}^{\rho_+} \frac{d\rho}{j(\rho)-j^*} = \frac{1}{\nu}\int_0^L dx = L/\nu. \tag{17}$$

In the limit $L\to\infty$, the left-hand side has to become divergent. This condition determines the steady-state current j^* and one recovers the extremal principle (5). It is important to note that the argument is independent of the value of ν and, indeed, of the precise form of $j_{\rm ex}$ [6,7].

The same result could be obtained by taking $\nu\to 0$ and keeping the system size L fixed. In the continuum approach, ν plays the role of a viscosity that prevents the occurrence of instabilities well known, e.g., for the inviscid Burgers equation $\partial_t\rho = -\partial_x\rho(1-\rho)$ that one obtains rigorously [31] from the TASEP in which $j=\rho(1-\rho)$. Adding the viscosity term $\nu\partial_x\rho$ to the Burgers equation [32], but setting the viscosity ν to zero, yields solutions with stable shocks of width $\propto 2\nu\to 0$. It is intriguing that an infinitesimal viscosity term (proportional to the lattice constant) appears when taking the ''naive'' continuum limit $k\to x=ka$, $t\to t'=ta$ of the lattice continuity equation (10) for the TASEP and keeping all terms to first order in the lattice constant a. For the TASEP, one has $j_k=\langle 10\rangle_{k,k+1}$. Due to the lack of correlations in the steady state, one may write in the mean-field approximation $j_k=\rho_k(1-\rho_{k+1})$ and then find from the Taylor expansion

$$\frac{\partial}{\partial t'}\rho = -\frac{\partial}{\partial x}\rho(1-\rho) + \frac{a}{2}\frac{\partial^2}{\partial x^2}\rho. \tag{18}$$

This suggests a shock width for the TASEP of the order of the lattice constant a, in agreement with known rigorous results [34,35]. Our previous discussion of the phase diagram suggests that such an infinitesimal viscosity term (also known as diffusive excess current) is a generic feature of the behavior of driven diffusive systems on the Euler scale. In the macroscopic description, it prevents the occurrence of instabilities (which cannot occur in a driven diffusive system on the lattice) and at the same time leads to shocks of zero width (i.e., proportional to the lattice constant) for systems with short-range interactions and short-range correlations in the steady state.

IV. UNIVERSAL PROPERTIES OF THE BOUNDARY LAYER

Our derivation of the asymptotic behavior of the density profile in the maximum- and minimum-current phases relies on a continuum description of density fluctuations $\phi(x,t)$ around a state of uniform mean density $\overline{\rho}$. Expanding the hydrodynamic equation (13) to second order in ϕ and adding phenomenological diffusion and noise terms, one arrives at the well-known noisy Burgers-Kardar-Parisi-Zhang (KPZ) equation [13,22,36–39],

$$\frac{\partial\phi}{\partial t} = \nu\frac{\partial^2\phi}{\partial x^2} - v_c(\overline{\rho})\frac{\partial\phi}{\partial x} - \lambda\phi\frac{\partial\phi}{\partial x} - \frac{\partial\eta}{\partial x}. \tag{19}$$

Here $\lambda = d^2j/d\rho^2(\overline{\rho})$ and $\eta(x,t)$ is Gaussian white noise in space and time representing the fast degrees of freedom. The noise strength D is defined through the covariance

$$\langle \eta(x,t)\,\eta(x',t')\rangle = D\,\delta(x-x')\,\delta(t-t'). \tag{20}$$

In the usual application to translationally invariant systems, the drift term $v_c\partial\phi/\partial x$ is eliminated by going to a comoving frame.

An important property of the one-dimensional KPZ equation is the invariance of the parameters λ and D/ν under renormalization (i.e., a change of measurement scale). The invariance of λ is a consequence of the Galilean symmetry of Eq. (19), which holds in all dimensions, while the invariance of D/ν results from a fluctuation-dissipation relation specific to the one-dimensional case [36]. The existence of these two invariants implies that the scaling properties of spatiotemporal fluctuations can be deduced from dimensional analysis. Moreover, for $v_c=0$ all correlation functions can be reduced

to a universal, system-independent form by an appropriate rescaling, which involves only the invariant quantities λ and D/ν [40].

In the following, this type of reasoning will be applied to the open system. Due to the presence of spatially fixed boundaries, the drift term then cannot be eliminated, and its effects are, as we have seen, highly nontrivial. However, in the maximum- and minimum-current phases, $v_c=0$. The only quantities that could enter a possible length scale characterizing the boundary layer are therefore λ, D/ν, and the relevant boundary density or, more precisely, its deviation, $\Delta\rho=\rho_{\pm}-\rho_{\rm bulk}$ from the bulk density. As the dimension of λ contains the dimension of time, it cannot enter a stationary quantity, and we are left with D/ν and $\Delta\rho$. The only combination with the dimension of length is

$$l_b=(D/\nu)(\Delta\rho)^{-2}, \tag{21}$$

and we conclude that the density profile must be of the form [6] (we assume the boundary to be located at $x=0$)

$$\langle\phi(x)\rangle=\Delta\rho\mathcal{F}(x/l_b), \tag{22}$$

where the universal scaling function $\mathcal{F}$ satisfies $\mathcal{F}(0)=1$ and vanishes for large arguments.

Let us now postulate, in addition, that the density profile becomes independent of the boundary density for $x\gg l_b$. This is plausible because in the maximum- and minimum-current phases, there is no mechanism for propagating boundary information into the bulk, which can be seen clearly also in the directed polymer formulation of the problem [41]. Then the asymptotic behavior of $\mathcal{F}$ has to be such as to cancel the factor $\Delta\rho$ on the right-hand side of Eq. (22), and it follows that $|\langle\phi(x)\rangle|\approx c^*(D/\nu)^{1/2}x^{-1/2}$ with some universal constant c^*.

It remains to identify the physical meaning of D/ν and the value of c^*. To accomplish the first task, we note that the stationary height difference correlation function of the one-dimensional KPZ equation is given by [22,40]

$$\langle[h(x)-h(x')]^2\rangle=(D/2\nu)|x-x'|. \tag{23}$$

In the present notation, the height $h(x)$ is the spatial integral of ϕ, hence $h(x)-h(x')$ is the fluctuation in the number of lattice-gas particles between x and x'. We conclude that D/ν is proportional to (a nonequilibrium analog of) the compressibility κ, which characterizes the mean-square deviation of the number N of particles in a sufficiently large volume L and is defined through

$$\kappa=\lim_{L\to\infty}\frac{\langle N^2\rangle-\langle N\rangle^2}{L}. \tag{24}$$

For the process (1)–(4), κ is readily computed using Eq. (A1), and one obtains

$$\kappa=\rho(1-\rho)\sqrt{1+4\rho(1-\rho)\left(\frac{1-\epsilon}{1+\epsilon}-1\right)}. \tag{25}$$

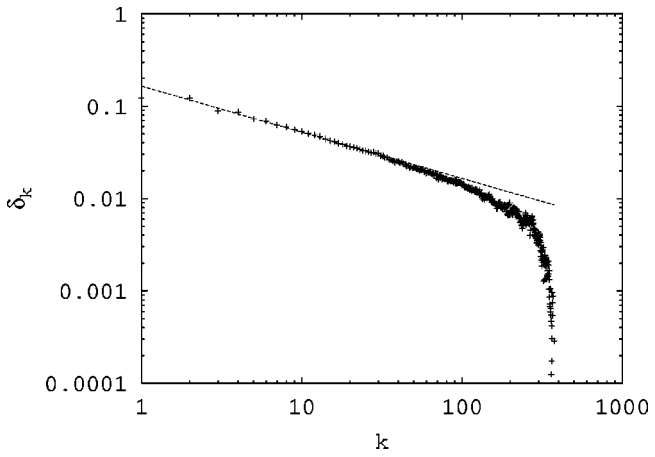

FIG. 7. Deviation δ_k for the maximal-current phase. The parameters are as in Fig. 1, with $\rho_-=1,\rho_+=0.45$. The system has 1000 sites and averaging is done over 3×10^6 Monte Carlo steps. The straight line shows the prediction of the universality hypothesis.

In particular, for the TASEP, $\kappa=\rho(1-\rho)$. Using this expression, the value of the universal amplitude c^* can be read off from the exact solution of the TASEP density profile [8,9]. Putting everything together, we arrive at the central conjecture of this section, which states that for any one-dimensional lattice-gas model in a maximum- or minimum-current phase, the deviation of the density profile from the bulk value $\delta_k=|\langle n_k\rangle-\rho_{\rm bulk}|$ decays asymptotically as

$$\delta_k=\sqrt{\kappa/\pi k}. \tag{26}$$

Numerical results for the density profile created by the process (1)–(4), shown in Figs. 7 and 8, are found to confirm the conjecture (26). It is further verified by the exact solutions of the TASEP with parallel update [10,11] and of the partially asymmetric simple exclusion process [12]. In the latter case, Eq. (26) implies, surprisingly, that the asymptotic density profile is independent of the asymmetry

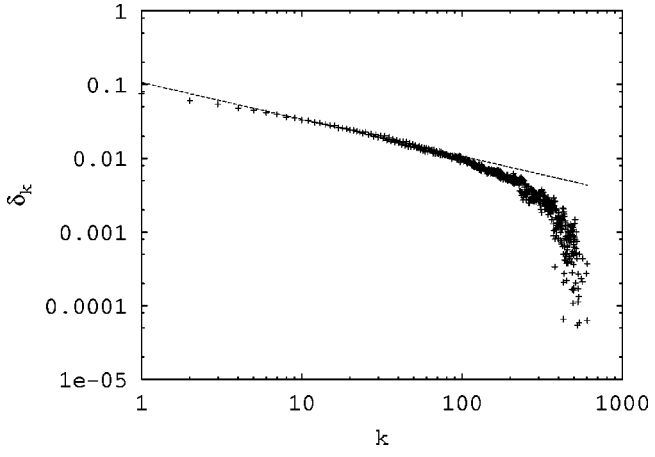

FIG. 8. Deviation δ_k for the minimal-current phase, with $\epsilon=0.96,\delta=0$ and boundary densities $\rho_-=0.4,\rho_+=0.6$. The system size and statistics are as in Fig. 7. The straight line shows the prediction of the universality hypothesis.

(provided it is nonzero), since the bias does not affect the compressibility.

It does, however, affect the length scale beyond which the asymptotic behavior sets in. For small bias, one expects an intermediate range where the density profile follows the $1/x$ decay predicted by mean-field theory [6]. More precisely, from the mean-field stationarity condition (15), one obtains the decay law $|\rho-\rho_{\rm bulk}|\approx\nu/\lambda x$, which sets in beyond the mean-field boundary scale $l_b^{\rm MF}=\nu/(\lambda\Delta\rho)$. The mean-field profile matches the asymptotic behavior (26) at the length scale $l_{\rm KPZ}=\nu^3/(D\lambda^2)$, which quite generally describes the crossover from diffusive to KPZ scaling behavior [40]. Since for the partially asymmetric exclusion process λ is proportional to the asymmetry, we see that $1\ll l_b^{\rm MF}\ll l_{\rm KPZ}$ for vanishing bias. It would be interesting to extract this scaling scenario from the exact solution of the partially asymmetric model [12,42].

In fact, the validity of our conjecture may extend beyond the class of driven diffusive systems with open boundaries. The exact form (26) of the density profile has been found also in the related problem of an asymmetric exclusion process with a moving impurity, in the phase where the impurity moves at the same speed as the density fluctuations (corresponding to the condition $v_c=0$) [43,44]. It is therefore conceivable that Eq. (26) applies generally in situations where a fluctuating noisy Burgers field is perturbed locally in such a way that the disturbance is stationary in the frame of the density fluctuations.

V. SIMULATION OF THE KLS MODEL

To check the theoretical predictions, we have simulated the two-parameter KLS model for a generic value $\delta=0.2,\epsilon=0.995$ of the coupling constants, chosen such that one has two maxima and one minimum in the current-density relation. As we are studying the open system, the injection/extraction mechanism at the boundaries has to be specified. It is a subtle point deserving special attention. It is the boundary that induces the phase transitions in driven systems. So the latter are extremely ''boundary-dependent.'' Because of the particle interaction, coupling of a semi-infinite system to a reservoir will generically lead to some discontinuous behavior of the stationary distribution close to the boundary. This is completely independent of any interaction with the bulk dynamics. The boundary represents an inhomogeneity of the system since the interaction of the particles with the fixed boundary leads to different correlations from those that result from the interaction of particles among themselves. The result are effective boundary densities $\rho_\pm$, which in general may differ from the reservoir densities $\hat\rho_\pm$ and which are not controlled by the interaction with the bulk. This is a nonuniversal phenomenon that depends on the precise nature of the coupling mechanism and on the nature of the particle interaction.

Given two reservoir densities, there is no general recipe for how to eliminate the nonuniversal boundary effects that result in the effective boundary densities ρ_-,ρ_+ that enter the theoretical description of the previous sections. Hence these quantities are not easy to control. Ideally, for the purpose of theoretical investigation, one would like to construct an injection and absorption mechanism that leads to a constant density profile for a semi-infinite system so that the effective boundary densities are identical to the real boundary densities $\hat\rho_\pm$, which determine the injection/absorption rates and hence are the actual control parameters of the model. For the KLS model, we choose an injection mechanism where the particles on the lattice interact with the reservoir particles in the same way as among each other. Such a mechanism can be constructed following Ref. [27]. This choice of boundary conditions has a nice property: If $\rho_-=\rho_+$, the exact stationary measure can be found. It is the Ising measure (A1) for a nonperiodic system with boundary fields, see Appendix B.

The continuous-time dynamics of the process are modeled by a random sequential update where first a site number x in the interval $[1,L]$ is chosen at random. If it contains a particle, the hopping is attempted with the rates (1)–(4) ($1\leqslant x\leqslant L-2$) or Eqs. (B3)–(B5) (if $x=L$ or $x=L-1$). If site 1 is chosen and empty, injection of a particle is attempted with rates (B1) and (B2). The rates are normalized with respect to the largest one, in our case $1+\epsilon$. This procedure, repeated L times, constitutes one Monte Carlo step. We performed Monte Carlo simulations for systems of sizes L from 100 to 1000. Densities and currents were averaged over at least $50L$ rounds, and averaged over seven different histories. The location of the first-(second-) order transition was determined by the appearance of a peak (jump) in the first derivatives of the bulk density $\rho_{\rm bulk}(\rho^+,\rho^-)$ with respect to ρ^+ and ρ^-. As an initial state, we chose either the empty or the completely filled lattice, whichever gave the faster convergence. Despite finite-size effects, the precise analysis of which requires further investigations, the overall agreement of the simulated phase diagram with the predicted one is very good already for $L=150$ (Fig. 2).

VI. CELLULAR AUTOMATA WITH DETERMINISTIC BULK DYNAMICS

The KLS model and indeed most lattice-gas models studied in the literature (see [23,24,45,46,31] for an overview) have stochastic bulk dynamics. On the other hand, the theoretical arguments discussed above do not really make use of the random nature of the dynamical rules. The shock velocity (7) and the collective velocity (8), which determine the phase diagram of open systems, are defined also for deterministic cellular automata. They depend on the dynamical rules only through the precise functional form of the current $j(\rho)$.

Therefore, it is not surprising that the phase diagram of lattice-gas models with deterministic bulk update and a single maximum in the current-density relation (but random injection at the boundaries to mimic the coupling to boundary reservoirs with variable densities) [47,48,10,11] is found to be correctly predicted by the extremal principle (5). In these models, there is no maximal-current phase [7], or, more precisely, the maximal-current phase reduces to a single point corresponding to the specific value of the boundary densities at which the current has its maximum. In [47],

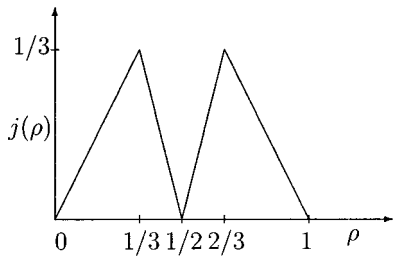

FIG. 9. Current-density relation of the deterministic cellular automaton (27)–(30).

we argued heuristically that this results from an overfeeding effect that cannot occur for deterministic bulk dynamics, i.e., the effective boundary densities cannot exceed the value where the collective velocity changes its sign and hence the maximal-current phase sets in.

This notion is in agreement with the prediction (26) for the amplitude of the hypothetical density profile in the maximal-current phase. In the models with deterministic bulk dynamics studied so far, the states with extremal current are characterized by a flat density profile and a fixed (i.e., nonfluctuating) number of particles. For such a state, however, Eq. (24) yields an amplitude $\kappa=0$, in agreement with the exact results.

In order to investigate the validity of the theoretical arguments in a setting with two maxima in the current-density relation, we consider the following cellular automaton, which has next-nearest-neighbor interactions as in the repulsive KLS model with $\epsilon=0$, but is defined by a deterministic, discrete-time update. Particles are driven to the right according to the rules

$$1100\rightarrow 1010 \quad \text{with probability } 1, \tag{27}$$

$$1101\rightarrow 1011 \quad \text{with probability } 1, \tag{28}$$

$$0100\rightarrow 0010 \quad \text{with probability } 1, \tag{29}$$

$$0101\rightarrow 0011 \quad \text{with probability } 0, \tag{30}$$

We use a parallel update in which first one determines for each particle whether it is allowed to move. Then all allowed moves are performed. It is straightforward to see by inspection of the periodic system that this gives a piecewise linear current density relation with two maxima and also one local minimum. One has a maximal current $j=\frac{1}{3}$ for the densities $\rho=\frac{1}{3}$ and $\rho=\frac{2}{3}$. The nearest-neighbor repulsion leads to a zero current state (. . . 010101 . . .) at density $\rho=\frac{1}{2}$ (Fig. 9).

The creation rates $\{\alpha\}$ at the left boundary and the annihilation rates $\{\beta\}$ at the right boundary are chosen as

$$1|00\rightarrow 1|10 \quad \text{with rate } \alpha, \tag{31}$$

$$1|01\rightarrow 1|11 \quad \text{with rate } \alpha, \tag{32}$$

$$11|0\rightarrow 10|0 \quad \text{with rate } \beta, \tag{33}$$

$$01|0\rightarrow 00|0 \quad \text{with rate } \beta. \tag{34}$$

The hopping rates of the leftmost and the next to rightmost site are governed by the bulk rules in conjunction with the constant dummy boundary sites added in Eqs. (31)–(34).

For $\alpha=\beta=1$ and an empty initial state, the system with $L=3K$ sites settles into a simple stationary state that gives weight $\frac{1}{3}$ to the three configurations 101001001 . . . 001, 110010010 . . . 010, and 010100100 . . . 100, respectively. This state has maximal current $j=\frac{1}{3}$ and an essentially flat density profile with local densities $\rho(1)=\rho(2)=\frac{2}{3}$, $\rho=\rho(x)=\frac{1}{3}$ for $2<x\leqslant L$. By particle-vacancy symmetry and space reflection, one obtains a similar stationary state with bulk density $\rho=\frac{2}{3}$. Numerical simulations and analytical results described elsewhere [49] show that there are no extremal current phases in any extended interval of α and β. The minimal current state is unstable for the boundary mechanisms (31)–(34) for any value of the rates α, β. It could be stabilized by a mechanism that for some value of the injection/absorption probabilities would leave the zero-current states 01010101 . . . 01 or 101010 . . . 10 invariant.

The relationship between the effective boundary densities and the rates α,β is surprisingly transparent. By changing the injection rate α of the model, one covers those effective left boundary densities that correspond to positive collective velocity [49]. Also in this model there is no overfeeding mechanism that would make effective left boundary densities corresponding to negative collective velocity accessible. Similarly, right boundary densities corresponding to positive collective velocities are inaccessible. The states of extremal current ($\rho=0$, $\frac{1}{3}$, $\frac{1}{2}$, $\frac{2}{3}$, and 1) have no finite fluctuations in the number of particles. The flat profile of the maximal current phases is consistent with the expression (24) for the amplitude of the density profile.

VII. EXCLUSION WITH PARTICLEWISE DISORDER

A distinguishing feature of the deterministic dynamics discussed in the preceding section is that it tends to give rise to singularities (slope discontinuities) in the current-density relation $j(\rho)$. A similar effect can be achieved by introducing quenched disorder into the system [50]. Specifically, let us consider a totally asymmetric exclusion process where each particle i is supplied with its own intrinsic jump rate p_i, which is a quenched random variable drawn from some distribution $f(p)$. If $p_i\geqslant c>0$ for all i and the distribution behaves as

$$f(p)\sim(p-c)^{\mu} \tag{35}$$

for $p\rightarrow c$, then for $\mu>0$ the system undergoes a phase transition to a spatially inhomogeneous *platoon phase* below a critical density ρ^* [51,52]. Here a platoon refers to a queue of particles trailing an exceptionally slow one. The current-density relation is linear for $\rho<\rho^*$ and singular at $\rho=\rho^*$. For $\mu\leqslant 1$, it can be shown that the critical density is always located below the density $\rho_{\max}$ at which the current attains its maximum, whereas for $\mu>1$, ρ^* and $\rho_{\max}$ can be made to coincide.

The question then arises to what extent such a singularity at $\rho_{\max}$ affects the phase diagram of the open system, and, in

particular, the density profile in the maximum-current phase. In a recent numerical study of the open TASEP with particlewise disorder, the usual $1/\sqrt{x}$ decay of the density profile was found [53]. This is surprising from the point of view of mean-field theory, which predicts a direct relation between the asymptotic density decay and the order of the maximum of the current function $j(\rho)$ [6]. In view of the considerations of Sec. IV, however, we see that the relevant feature is not the behavior of $j(\rho)$, but rather the compressibility κ. As we show in the following, κ remains finite at the platoon phase transition when $\mu>1$, and therefore a conventional $1/\sqrt{x}$ decay of the density profile should indeed be expected.

The steady state of the TASEP with particlewise disorder and periodic boundary conditions consists of a product measure for the particle headways $u_i=x_{i+1}-x_i-1$, which count the number of vacant sites in front of particle i (x_i denotes the position of particle i). The distribution of u_i is geometric, with a parameter depending on the particle jump rate p_i and the overall density ρ [51,52]. The compressibility is related to the variance of the headways through the relation

$$\kappa=\rho^3\overline{(\langle u_i^2\rangle-\langle u_i\rangle^2)}, \tag{36}$$

where angular brackets refer to an average over the stochastic dynamics and the overbar denotes the average with respect to the disorder in the jump rates. Equation (36) can be derived from a simple central limit argument. At the platoon phase transition, the disorder-averaged headway distribution decays as a power law, as $u^{-(\mu+2)}$ [51], and therefore the right-hand side of Eq. (36) remains finite when $\mu>1$.

Explicit formulas for κ can be obtained using the results of Refs. [51,52] for the disorder distribution,

$$f(p)=\frac{\mu+1}{(1-c)^{\mu+1}}(p-c)^{\mu}, \quad c\leqslant p\leqslant 1. \tag{37}$$

For random sequential dynamics, one finds

$$\kappa(\rho^*)=\frac{\mu^3(\mu+1)c(1-c)^2}{(\mu+c)^3}\left(\frac{1}{\mu}+\frac{c}{(\mu-1)(1-c)}\right), \tag{38}$$

while for parallel update

$$\kappa(\rho^*)=\frac{\mu^2(\mu+1)c}{(\mu+c+\mu c)^3}\left(1-\frac{c(\mu-2)}{\mu-1}\right). \tag{39}$$

For the case considered in [53] (parallel update with $\mu=2$ and $c=0.4$), Eqs. (26) and (39) yield a prefactor for the density profile that is about 40% larger than the numerical estimate. It seems worthwhile to carry out more precise simulations to determine whether this discrepancy implies a breakdown of universality due to the quenched disorder.

VIII. CONCLUSIONS

The interplay of density fluctuations and shock diffusion, and coalescence and branching, respectively, as described above represents the basic mechanisms that determine the steady-state selection of driven diffusive systems with two maxima in the current-density relation. The phase diagram for systems with short-ranged interactions is generic. Hence knowledge of the macroscopic current-density relation $j(\rho)$ of a given physical system is sufficient to calculate the exact nonequilibrium phase transition lines in terms of effective boundary densities $\rho_{\pm}$. The effective left boundary density depends in a nonuniversal manner only on the left boundary coupling mechanism, while the effective right boundary density depends only on the right boundary coupling mechanism. A surprising phenomenon is the occurrence of the self-organized minimal-current phase.

In all extremal current phases, the amplitude of the density profile is determined by the nonequilibrium analog κ of the compressibility. For lattice-gas models without particle number fluctuations, this implies a flat density profile. This is consistent with older exact results on deterministic systems with a single maximum in the current-density relation and the numerical study of the cellular automaton with two maxima of the current that we have considered here. It appears that the absence of an extremal current phase, a flat profile in the points of extremal current, and the absence of particle number fluctuations are a characteristic property of models with deterministic bulk dynamics, but stochastic injection and absorption at the boundaries.

The investigation of the motion of perturbations and of the stability and motion of shocks in the framework of the stochastic lattice-gas description also yields a ''mesoscopic'' derivation of the large-scale hydrodynamic description of the lattice-gas dynamics in the scaling regime $u=x/t$. This rather general conclusion is supported by rigorous proofs of the validity of the hydrodynamic description for specific models [45,31]. In the case of multicomponent systems, the situation is much more complicated even in one dimension. There is no unique way of ''regularizing'' the continuum version of the lattice continuity equation by a diffusive current as in Eq. (14). The investigation of multicomponent lattice-gas models could provide a clue as to which kind of mechanism is responsible for boundary-driven phase transitions.

ACKNOWLEDGMENTS

We thank T. Antal, C. Bahadoran, and O. Zaboronski for useful discussions. V.P. acknowledges financial support by the Alexander–von Humboldt Stiftung. J.K. acknowledges the hospitality of the Erwin Schrödinger Institute for Mathematical Physics, where his contribution to this work was begun.

APPENDIX A: STEADY-STATE PROPERTIES OF THE KLS MODEL

The model investigated here is a special case in the class of driven diffusive systems investigated in Ref. [5]. On a ring with L sites with periodic boundary conditions, the stationary distribution turns out to be given by the equilibrium distribution of the one-dimensional Ising model. Let us denote a configuration of the system by the sequence of occupation numbers $\{n_i\}_{i=1}^{L}$, where $n_i=1$ if there is a particle at

site i; otherwise, $n_i=0$. Then, the unnormalized probability of a steady-state configuration $\{n_i\}_{i=1}^L$ is given by the Ising distribution

$$P_{\{n_i\}}=e^{-\beta\Sigma_{n=1}^{L}(1-2n_i)(1-2n_{i+1})-h\Sigma_{i=1}^{L}(1-2n_i)}/Z \quad \text{(A1)}$$

with the partition function

$$Z=\sum_{\text{all } n_j} P_{\{n_j\}} \quad \text{(A2)}$$

and $\exp(4\beta)=(1+\epsilon)/(1-\epsilon)$. The field strength h acts as a chemical potential, fixing the bulk density ρ.

Therefore, all the averages can be computed using the standard transfer-matrix technique (see, e.g., [54]). One introduces a 2×2 transfer matrix

$$V=\begin{pmatrix} e^{-\beta-h} & e^{\beta} \\ e^{\beta} & e^{-\beta+h} \end{pmatrix} \quad \text{(A3)}$$

such that $\mathrm{Tr}(V^L)=Z$. Then, the probability of finding a particle at a given site is given by $\rho=\langle 1\rangle=\mathrm{Tr}(AV^{L-1})/Z$ with

$$A=\begin{pmatrix} 0 & 0 \\ 0 & 1 \end{pmatrix} V. \quad \text{(A4)}$$

Analogously, for the hole one calculates $\langle 0\rangle=\mathrm{Tr}(BV^{L-1})/Z$, where $B=V-A$, ensuring $\langle 0\rangle+\langle 1\rangle=1$. Correlation functions are calculated by the trace over products of the matrices A,B,V, e.g., $\langle 1100\rangle=\mathrm{Tr}(AABBV^{L-4})/Z$, and so on. Diagonalizing V, and taking the thermodynamic limit $L\to\infty$, one obtains for the average density of particles

$$\rho=\frac{1}{2}\left(1+\frac{e^{-2\beta}\sinh(h)}{\sqrt{1+e^{-4\beta}\sinh^2(h)}}\right) \quad \text{(A5)}$$

in terms of the chemical potential.

We stress that the existence of an equilibrium distribution as a stationary measure does *not* mean that the particle hopping model approaches thermal equilibrium (in the physical meaning of the notion) at long times. The reason is that the stationary distribution does not satisfy detailed balance with respect to the dynamics of the model. The nonequilibrium nature of the steady state results in a nonvanishing stationary particle current (11). One obtains in the thermodynamic limit

$$j=\frac{\lambda[1+\delta(1-2\rho)]-\epsilon\sqrt{4\rho(1-\rho)}}{\lambda^3} \quad \text{(A6)}$$

with the largest eigenvalue λ of the transfer matrix V,

$$\lambda=\frac{1}{\sqrt{4\rho(1-\rho)}}+\left(\frac{1}{4\rho(1-\rho)}-1+\frac{1-\epsilon}{1+\epsilon}\right)^{1/2}. \quad \text{(A7)}$$

For the simple exclusion process $\epsilon=\delta=0$, we recover the usual formula $j=\rho(1-\rho)$. In another limiting case, $\epsilon=1$, $\delta=0$, the current is $j=x(1-x)/(1+x)$, and $x=\sqrt{1-4\rho(1-\rho)}$. The current-density relation (A6) is plotted in Fig. 1 for several values of ϵ and δ.

APPENDIX B: COUPLING TO BOUNDARY RESERVOIRS

Technically, it is easiest to think about two reservoirs of particles with the densities ρ_- and ρ_+, coupled to the left $i=1$ and the right $i=L$ end of the system, respectively. Both reservoirs are kept at the stationary state. The injection of a particle at site 1 is possible if site 1 is empty, but depends on the occupation of site 2, because the next-nearest interactions are present. It may be helpful to imagine the reservoir to include a site 0 of the chain. The injection rate into the first site is defined by the (stationary) average occupation ρ_- of the imaginary site 0, but with the condition that the first site is empty and the second site is occupied. Considering the zeroth, the first, and the second site as three neighboring sites of an infinite chain, this conditional probability can be expressed readily as correlations in the stationary state of an infinite chain.

Applying a similar reasoning to the right boundary reservoir, one obtains the following scenario. If sites 1 and 2 are both empty, a particle from the left reservoir ρ_- hops onto site 1 with the rate, averaged between the corresponding bulk rates (1)–(4):

$$\frac{(1+\delta)\langle 0100\rangle_{\rho_-}+(1+\epsilon)\langle 1100\rangle_{\rho_-}}{\langle 00\rangle_{\rho_-}}=\mathbf{P}, \quad |00\overset{\mathbf{P}}{\rightarrow}|10, \quad \text{(B1)}$$

where, e.g., $\langle 100\rangle_\rho$ is a stationary-state probability of a configuration 100 in an infinite system with average density ρ. Similarly, if site 1 is empty and site 2 occupied, the injection rate is

$$\frac{(1-\delta)\langle 1101\rangle_{\rho_-}+(1-\epsilon)\langle 0101\rangle_{\rho_-}}{\langle 01\rangle_{\rho_-}}=\mathbf{Q}, \quad |01\overset{\mathbf{Q}}{\rightarrow}|11. \quad \text{(B2)}$$

The extraction rates at the right end are determined analogously, with a difference being that averages are now taken at a density ρ_+:

$$\frac{(1+\delta)\langle 0100\rangle_{\rho_+}+(1-\epsilon)\langle 0101\rangle_{\rho_+}}{\langle 01\rangle_{\rho_+}}=\mathbf{R}, \quad 01|\overset{\mathbf{R}}{\rightarrow}00|, \quad \text{(B3)}$$

$$\frac{(1-\delta)\langle 1101\rangle_{\rho_+}+(1+\epsilon)\langle 1100\rangle_{\rho_+}}{\langle 11\rangle_{\rho_+}}=\mathbf{S}, \quad 11|\overset{\mathbf{S}}{\rightarrow}10|. \quad \text{(B4)}$$

We shall see below that the seemingly complicated choice of the rates is fully justified by the remarkable property it possesses. But first notice that Eqs. (B1)–(B4) do not specify the rates completely, because the particle at the sites 1 and $L-1$ will still feel the presence of the reservoir. Therefore, in addition to Eq. (B1), we should specify the rate of the processes

$$|100\rightarrow|010, \quad |101\rightarrow|011, \quad 110|\rightarrow 101|, \quad 010|\rightarrow 001|.$$

This is done in a similar way, e.g., the first process has the rate

$$\frac{(1+\epsilon)\langle 1100\rangle_{\rho_-}+(1+\delta)\langle 0100\rangle_{\rho_-}}{\langle 100\rangle_{\rho_+}}=\mathbf{P}_1, \quad \overset{\mathbf{P}_1}{|100\rightarrow|010} \tag{B5}$$

and the three remaining rates are written analogously. Note that for the simple exclusion model $\epsilon=\delta=0$, the correlations are absent, $\langle 10\rangle=\langle 1\rangle\langle 0\rangle=\rho(1-\rho)$, and the above rates simply reduce to the usual ones $|0\rightarrow|1$ with rate ρ_- and $1|\rightarrow 0|$ with rate $1-\rho_+$.

The above choice of the injection/extraction rates Eqs. (B1)–(B5) possesses a nice property. Namely, when $\rho_-=\rho_+=\rho$, the stationary-state probability can be found exactly: it is the Ising distribution Eq. (A1) of an open chain with bulk and boundary fields:

$$P_{\{n_i\}}=e^{-\beta H_{\mathrm{Ising}}^{\mathrm{open}}-h\Sigma_{i=1}^{L}(1-2n_i)+g(n_1+n_L-1)}/Z, \tag{B6}$$

where

$$H_{\mathrm{Ising}}^{\mathrm{open}}=\sum_{i=1}^{L-1}(1-2n_i)(1-2n_{i+1}) \tag{B7}$$

and the strength of the boundary field g is given by

$$e^h-e^{-h}=e^{2\beta}(e^{g+h}-e^{-g-h}). \tag{B8}$$

This statement is verified directly, substituting the rates Eqs. (B1)–(B4) in the stationarity condition; see, e.g., [27].

We note that expectation values for the distribution (B6) are calculated with the same transfer matrix as in the periodic case. However, instead of taking a trace, one calculates a scalar product with suitably chosen vectors, which are determined by the boundary fields. Taking any finite lattice of size $L\geqslant 3$, and computing the average occupation numbers $\langle n_i\rangle$, using the stationary-state probabilities (B6), one gets the constant density $\langle n_1\rangle=\langle n_2\rangle=\cdots=\langle n_N\rangle$, *provided* Eq. (B8) is satisfied. Thus, applying the injection/extraction rates Eqs. (B1)–(B4) guarantees inducing effective boundary densities ρ_-,ρ_+ on the left and on the right boundary, respectively.

[1] *Nonequilibrium Statistical Mechanics in One Dimension*, edited by V. Privman (Cambridge University Press, Cambridge, 1997).
[2] B. C. Eu, *Nonequilibrium Statistical Mechanics* (Kluwer, Dordrecht, 1998).
[3] A. B. Kolomeisky, G. M. Schütz, E. B. Kolomeisky, and J. P. Straley, J. Phys. A **31**, 6911 (1998).
[4] V. Popkov and G. M. Schütz, Europhys. Lett. **48**, 257 (1999).
[5] S. Katz, J. L. Lebowitz, and H. Spohn, J. Stat. Phys. **34**, 497 (1984).
[6] J. Krug, Phys. Rev. Lett. **67**, 1882 (1991).
[7] J. Krug, in *Spontaneous Formation of Space-Time Structures and Criticality*, edited by T. Riste and D. Sherrington (Kluwer Academic, Dordrecht, 1991), p. 37.
[8] G. Schütz and E. Domany, J. Stat. Phys. **72**, 277 (1993).
[9] B. Derrida, M. R. Evans, V. Hakim, and V. Pasquier, J. Phys. A **26**, 1493 (1993).
[10] M. R. Evans, N. Rajewski, and E. R. Speer, J. Stat. Phys. **95**, 45 (1999).
[11] J. de Gier and B. Nienhuis, Phys. Rev. E **59**, 4899 (1999).
[12] T. Sasamoto, J. Phys. Soc. Jpn. **69**, 1055 (2000).
[13] H. K. Janssen and K. Oerding, Phys. Rev. E **53**, 4544 (1996).
[14] D. Helbing, *Verkehrsdynamik: Neue Physikalische Modellierungskonzepte* (Springer, Berlin, 1997).
[15] D. Chowdhury, L. Santen, and A. Schadschneider, Phys. Rep. **329**, 199 (2000).
[16] V. Popkov, L. Santen, A. Schadschneider, and G. M. Schütz, J. Phys. A **34**, L45 (2001).
[17] J. T. MacDonald, J. H. Gibbs, and A. C. Pipkin, Biopolymers **6**, 1 (1968).
[18] J. T. MacDonald and J. H. Gibbs, Biopolymers **7**, 707 (1969).
[19] V. Kukla, J. Kornatowski, D. Demuth, I. Girnus, H. Pfeifer, L. Rees, S. Schunk, K. Unger, and J. Kärger, Science **272**, 702 (1996).
[20] Q. H. Wei, C. Bechinger, and P. Leiderer, Science **287**, 625 (2000).
[21] H. Brandstetter, Diploma thesis, University of Munich, 1991 (unpublished).
[22] J. Krug and H. Spohn, in *Solids Far From Equilibrium*, edited by C. Godréche (Cambridge University Press, Cambridge, England, 1991).
[23] T. M. Liggett, *Stochastic Interacting Systems* (Springer, Berlin, 1999).
[24] G. M. Schütz, *Exactly Solvable Models for Many-body Systems far from Equilibrium*, in *Phase Transitions and Critical Phenomena*, edited by C. Domb and J. Lebowitz (Academic, London, 2000), Vol. 19.
[25] B. Derrida, Phys. Rep. **301**, 65 (1998).
[26] T. M. Liggett, Trans. Am. Math. Soc. **179**, 433 (1975).
[27] T. Antal and G. M. Schütz, Phys. Rev. E **62**, 83 (2000).
[28] K. Oerding and H. K. Janssen, Phys. Rev. E **58**, 1446 (1998).
[29] H. Fogedby, Phys. Rev. Lett. **80**, 1126 (1998).
[30] P. A. Ferrari, L. R. G. Fontes, and M. E. Vares, Ann. Inst. Henri Poincaré Phys. Theor. **36**, 109 (2000).
[31] C. Kipnis and C. Landim, *Scaling Limits of Interacting Particle Systems* (Springer, Berlin, 1999).
[32] M. Plischke, Z. Rácz, and D. Liu, Phys. Rev. B **35**, 3485 (1987).
[33] D. P. Ballou, Trans. Am. Math. Soc. **152**, 441 (1970).
[34] B. Derrida, J. L. Lebowitz, and E. R. Speer, J. Stat. Phys. **89**, 135 (1997).
[35] V. Belitsky and G. M. Schütz (unpublished).
[36] D. Forster, D. R. Nelson, and M. J. Stephen, Phys. Rev. A **16**, 732 (1977).
[37] H. van Beijeren, R. Kutner, and H. Spohn, Phys. Rev. Lett. **54**, 2026 (1985).
[38] H. K. Janssen and B. Schmittmann, Z. Phys. B: Condens. Matter **63**, 517 (1986).

[39] M. Kardar, G. Parisi, and Y. C. Zhang, Phys. Rev. Lett. **56**, 889 (1986).
[40] J. Krug, Adv. Phys. **46**, 139 (1997).
[41] J. Krug and L. H. Tang, Phys. Rev. E **50**, 104 (1994).
[42] R. A. Blythe, M. R. Evans, F. Colaiori, and F. H. L. Essler, J. Phys. A **33**, 2313 (2000).
[43] K. Mallick, J. Phys. A **29**, 5375 (1996).
[44] T. Sasamoto, Phys. Rev. E **61**, 4980 (2000).
[45] H. Spohn, *Large Scale Dynamics of Interacting Particles* (Springer, Berlin, 1991).
[46] B. Schmittmann and R. K. P. Zia, *Statistical Mechanics of Driven Diffusive Systems*, in *Phase Transitions and Critical Phenomena*, edited by C. Domb and J. Lebowitz (Academic, London, 1995), Vol. 17.
[47] G. Schütz, Phys. Rev. E **47**, 4265 (1993).
[48] L. G. Tilstra and M. H. Ernst, J. Phys. A **31**, 5033 (1998).
[49] J. S. Hager (unpublished).
[50] J. Krug, Braz. J. Phys. **30**, 97 (2000).
[51] J. Krug and P. A. Ferrari, J. Phys. A **29**, L465 (1996).
[52] M. R. Evans, J. Phys. A **30**, 5669 (1997).
[53] M. Bengrine, A. Benyoussef, H. Ez-Zahraouy, J. Krug, M. Loulidi, and F. Mhirech, J. Phys. A **32**, 2527 (1999).
[54] R. J. Baxter, *Exactly Solved Models in Statistical Mechanics* (Academic, New York, 1982).